Available online at www.sciencedirect.com
ScienceDirect
Proceedings of the Combustion Institute 000 (2018) 1–8
Proceedings of the Combustion Institute
www.elsevier.com/locate/proci

Examination of the electronic structure of oxygen-containing PAH dimers and trimers

Jennifer A. Giaccai, J. Houston Miller*

Department of Chemistry, The George Washington University, 800 22nd Street, NW, Suite 4000 Washington, DC 20052, USA

Received 30 November 2017; accepted 21 May 2018
Available online xxx

Abstract

Interactions of oxygen with polynuclear aromatic hydrocarbons (PAH) can occur both in the flame and during oxidation of soot atmospherically. Past experimental measurements of PAH in soot samples collected either immediately after combustion, from the atmosphere, or in a flame show a variety of oxygen moieties within the PAH structures. This study investigated the electronic structure of oxygen-containing PAH to gain insight into their interaction with light both to better interpret spectroscopic measurements and to recognize the role of oxygen-containing PAH in atmospheric radiative forcing. Our research has shown that oxygen in ethers and hydroxyl moieties on PAH showed little change to the HOMO-LUMO gap (HLG), whereas ketones and aldehydes show a HLG decrease of 0.5 eV. The effect is enhanced when more than one ketone is present on a PAH molecule and further enhanced in subsequent dehydrogenation to a quinone-like structure. The presence of an oxygen-containing PAH with a ketone functional group in a dimer and trimer will substantially lower the HLG of the PAH stack. This may have a significant effect in the interaction of atmospheric soot with solar radiation.

Keywords: Soot; Polynuclear aromatic hydrocarbons; Band gap; Oxidation; Electronic structure

1. Introduction

Black carbon (soot) absorbs a much greater portion of visible, solar radiation than any other atmospheric aerosols [1], leading to this class of particulates being second only to carbon dioxide as an atmospheric radiative forcer. Because the lifetime of black carbon in the atmosphere is relatively short compared to molecular greenhouse gases, it is thought that reduction of soot emissions will have a more immediate impact on climate forcing, allowing greater opportunity for the replacement of fossil fuels with carbon-neutral energy sources. Further, carbon quantum dots–essentially soot particulate with surfaces pacified with oxygen-containing functional groups–have been proposed as possible materials in solar radiation conversion due to their reported red-shifted band gaps compared to particulate with lower oxygen content. The unique optical properties of quantum dots have led to their proposed use as high

* Corresponding author.
E-mail address: giaccai@gwu.edu (J.A. Giaccai).

https://doi.org/10.1016/j.proci.2018.05.057
1540-7489

quantum yield fluorescent markers for biological imaging [2].

In studies of atmospheric soot particulate, Barradas-Gimate et al. were able to identify a large amount of anthra- and naphthaquinones in the PM2.5 [3]. The amount of quinones present changed depending on the season; the warm-dry season with greater solar radiation exposure resulted in greater amounts of quinones measured.

Past studies of soot have shown both the amount of oxygen present as well as the types of oxygen present in molecules can vary significantly depending on source. Schuster et al. showed that quinone formation was increased on the surface of diesel soot when oxidized some time after initial soot production [4]. Studies by vander Wal et al. of engine soots and other soots have shown that the amount of oxygen and the types of oxygen present in soot can vary depending on the power and type of a jet engine, the type of diesel fuel used in a diesel engine, as well as the source category, e.g., wildfire soot vs. oil burner [5,6]. The types of oxygen-containing hydrocarbons identified were carboxylic, carbonyl and hydroxyl groups; however ether/furan groups were not included in the fit of the X-ray photoelectron spectroscopy (XPS) peaks in these studies. XPS studies by Growney et al. primarily identified the presence of hydroxyl and ether/furan oxygen-containing hydrocarbons, with a small amount of carbonyl groups present in carbon black and diesel soot [7].

Recently, studies have focused on studying the carbon and oxygen speciation during soot formation [8–10]. Ouf et al. used synchrotron based NEXAFS and XPS to examine soot formed from a miniCAST both in an aerosol and collected as a sample. NEXAFS showed that carbonyl and carboxylic acid species could be identified on soot after collection, however the in situ XPS studies showed that ether or hydroxyl containing species were present on the surface of the particles in the aerosol phase. Modeling and experimental studies of the earliest stages of soot formation by Johannson et al. used XPS to determine nearly equal concentrations of ether and hydroxyl groups, with the hydroxyl groups decreasing and furan groups dominating later in the flame [9,10]. XPS studies of the reaction of coronene with oxygen have shown that PAH can easily form structures containing ether, carbonyl and carboxylic structures.

Other recent studies have investigated oxygen's role in the formation of 5-membered rings [11–15]. Oxidation at the edge of a graphene sheet primarily results in the formation of five-membered rings [15]. However some PAH survive with oxygens still present as a carbonyl or hydroxyl moiety on the PAH molecule [11]. Frenklach group studies demonstrated that OH oxidation of armchair sites is preferential to zigzag sites which is, in turn, more favorable than oxidation of free edge sites [12,13].

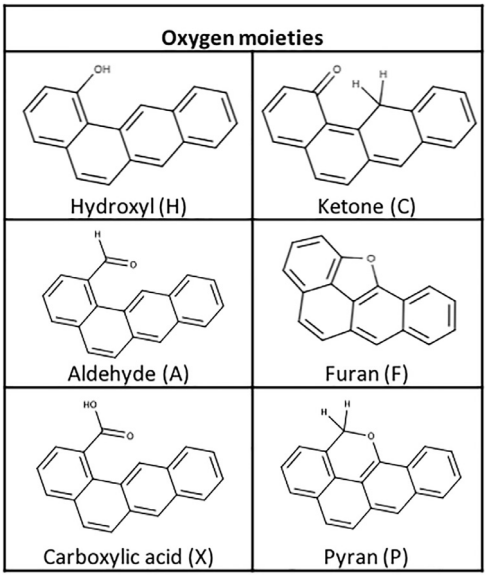

Fig. 1. Oxygen moieties used in this study. Oxygens are shown on benzanthracene in the outside (1) position. Hydrogens in ketone moiety are shown across the armchair from the ketone.

Chaparala and Raj have shown that oxygen is less likely to leave a zigzag site than a free edge [16].

Chen and Wang have recently examined the effect of oxygen substituents on the electronic structure of PAH, showing a decrease of the band gap when certain oxygen substituents are present [17]. Our group's previous investigations centered on the electronic structures of different PAH structures, including nearly circular, symmetric individual PAH molecules, PAH agglomerates and across different PAH topologies [18–20]. This paper extends these studies to the electronic structure of oxygen containing PAH, including molecules where oxygens are present as substituents, cyclic ethers and ketone groups in the PAH structure itself.

2. Methodology

Molecules were analyzed with density functional theory (DFT) with and without oxygen species. The parent molecules in the study are nine PAH molecules with at least one armchair feature ranging in molar mass from 178 Da (phenanthrene) to 643 Da (circumbenzo[*ghi*]perylene) and can be seen in Fig. S1. The oxygen moieties examined can be seen in Fig. 1. Abbreviations in the table are used in the chart showing DFT results for all molecules studies, presented in the Supplemental Information. Six different oxygen moieties were studied: three substituents onto a PAH [hydroxyl (OH), aldehyde (CHO) and carboxylic acids (COOH)]; two cyclic ethers [furans (COC-5) and

Please cite this article as: J.A. Giaccai, J.H. Miller, Examination of the electronic structure of oxygen-containing PAH dimers and trimers, Proceedings of the Combustion Institute (2018), https://doi.org/10.1016/j.proci.2018.05.057

pyrans (COC-6)]; and a ketone group directly on a PAH ring (C=O). Each oxygen moiety was added at the armchair edge of the parent molecule. In cases where the parent PAH molecule is asymmetric, both armchair edges were studied.

Adding a ketone to a PAH ring shifts one double bond outside of the PAH structure to the oxygen atom and forces sp^3 hybridization of one of the carbons in the PAH structure. Pyrans also contain an sp^3 hybridized carbon. Due to the aromaticity of the structure, the sp^3 hybridized carbon can occur in many locations on the PAH ring structure; this study only examined molecules with sp^3 carbons either immediately adjacent to the oxygen location or across the armchair from the ketone location.

Each monomer was geometry optimized in NWChem v 6.5 using density functional theory (DFT) with the 6–31G* basis set and B3LYP exchange correlation [21–24]. After geometry optimization, the DFT energies of the molecule and the partial charges on each atom were determined from the electrostatic potential. Although oxygen atoms have increased electronegativity, which might suggest the use of a basis set with diffuse components such as 6–31 + G*, tests showed that the differences in monomer geometries, dimer geometries and binding energies were minimal and did not justify the increase in computational time required when using the 6–31 + G* basis set. Dimers constructed from monomers optimized with 6–31 + G* (diffuse containing basis set) were examined and compared to the dimers used in the remainder of the study. Changes in binding energy (BE) averaged 1.3% greater with the diffuse 6–31 + G* basis set and can be seen in Fig. 2. Changes to the dimer geometries were minimal and can be seen in Fig. S3.

NWChem calculated Kohn-Sham orbitals were used to determine the HOMO-LUMO gaps (HLG) for monomers, dimers and trimers. For each oxygen moiety and parent PAH combination, the change in HLG between the parent PAH (ΔHLG) and the oxygen-containing PAH was calculated. To determine the overall effect of an oxygen moiety, the average and standard deviation of ΔHLG for each oxygen moiety was calculated across the various PAH parent molecules.

Dimers and trimers were not geometry optimized in NWChem, but rather PAH dimers and trimers were formed in a custom atom-pair minimization program that uses a simplex algorithm to find the geometric conformation of molecules with the strongest BE [25,26]. BE is calculated from the electrostatic and dispersive interactions between each atom on each molecule, Eq. (1).

$$BE = \sum_{i,j} q_i q_j r_{ij}^{-1} - A r_{ij}^{-6} + B e^{-C r_{ij}} \quad (1)$$

The electrostatic contribution is the coulombic potential between the partial charges (q) determined from NWChem on any two atoms (i,j)

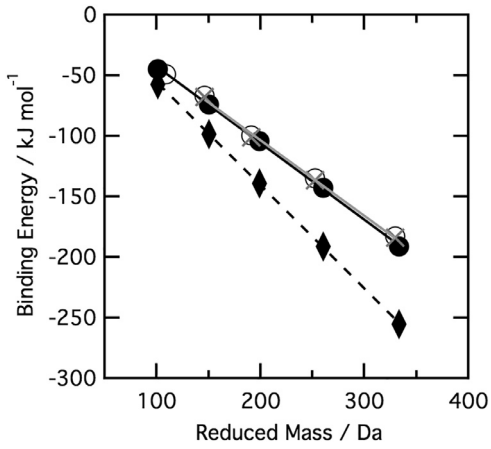

Fig. 2. Comparison of current and previous methods for evaluating the binding energy. Solid line and circles: W99 and ESP BE used in this work, open circles show oxygen-containing PAH. Dashed lines and diamonds: Herdman & Miller BE used in previous work. Gray lines and crosses: W99 and ESP BE calculated with 6–31 + G* basis set.

on the different molecules, while the dispersive potential is calculated from an exp-6 dispersive force using coefficients (A,B,C) determined by Williams (W99); r is the distance between the two atoms [27]. Our previous studies have shown that use of the partial charges calculated from the electrostatic potential field instead of assigning partial charges by atom type allows greater variety in the types of PAH molecules examined, including those with bays, fjords and alkyl sidechains that could not be previously studied [28]. Here, the use of partial charges derived from the electrostatic potential also allows for the inclusion of hetero atoms in the PAH.

Updating the dispersive coefficients A, B and C to the W99 coefficients allows the examination of PAH containing oxygen or nitrogen. The binding energies calculated with W99 are smaller than those calculated previously but follow the established trend with the BE proportional to the reduced mass of the dimer, see Fig. 2. Binding energies of both oxygen-containing PAH dimers and PAH dimers without oxygen are in agreement. Values of the binding energy of a coronene dimer obtained from calculations in other studies range from −73 to −98 kJ/mol [29–35], whereas our values using the W99 and JHM84 dispersive coefficients were −74 and −99 kJ/mol, respectively. W99 dispersive terms are prone to underestimating the BE in T-shaped conformers. While underestimating the BE may be problematic in studying larger PAH clusters, the lowest energy conformers for PAH dimers, as studied here, are turbostratic stacks [36].

Please cite this article as: J.A. Giaccai, J.H. Miller, Examination of the electronic structure of oxygen-containing PAH dimers and trimers, Proceedings of the Combustion Institute (2018), https://doi.org/10.1016/j.proci.2018.05.057

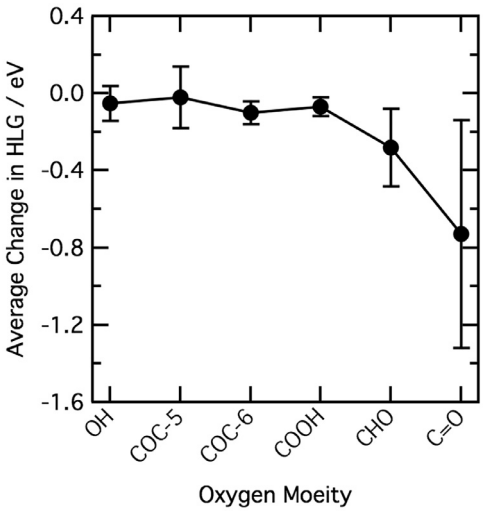

Fig. 3. Average ΔHLG from the parent molecule versus oxygen moiety for all singly-oxygenated PAH. Error bars show the standard deviation over the different parent PAH molecules studied. OH, CHO and COOH are hydroxyl, aldehyde and carboxylic acid substituents respectively. COC-5 and COC-6 are cyclic ethers with five or six membered rings, and C=O is a ketone group directly on a PAH ring.

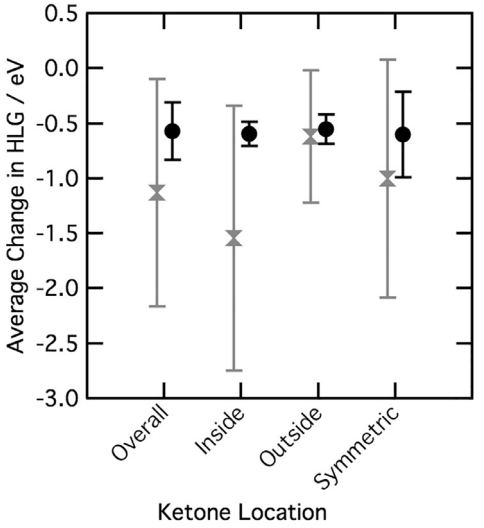

Fig. 4. Average change in HLG as the location of the ketone changes. Gray crosses: sp3 carbon located across the armchair from the ketone, black circles: sp3 carbon located adjacent to ketone. The ketone can be located on a symmetric PAH parent molecule, or towards the inside or outside of an asymmetric PAH parent molecule.

3. Results and discussion

3.1. Oxygen-containing PAH monomers

The oxygen moieties likely to be observed in the early PAH and soot formation regions; hydroxyls, furans and pyrans; show generally small changes in the HLG (see Fig. 3). The average and standard deviation were calculated for each moiety over all the parent molecules studied. A hydroxyl group substituent only shows an average change of −0.05 eV over all the molecules studied, while a furan shows an average change of −0.02 eV. Expected to be formed later in the flame, or in post-flame oxidation, aldehydes and ketones on the PAH ring on average show a decrease in the HLG. Although carboxylic acids show a negligible increase in the HLG (−0.07 eV), aldehydes show an average decrease of −0.28 eV and ketones on the PAH ring show an average decrease of −0.74 eV. When compared with the effect of the Boltzmann thermal energy distribution, kT at 1500 K is 0.13 eV, only the aldehyde substituent and ketones on the PAH ring can be considered to have significant effects on the HLG. Of the different oxygen moieties examined, only the ketone addition changes the π electron configuration of the PAH parent molecule.

For most molecules examined, locations where oxygen moieties were added were limited to armchair structures, due to their greater stability. However a small study of pyrene molecules was undertaken to ensure agreement with previous results of Chen and Wang [18]. When hydroxyl, carboxylic acid and aldehyde substituents were added to different locations of the pyrene molecule, our results generally agreed with those of Chen and Wang, see Supplemental Information. However, when examining the three possible locations that oxygen moieties could be located, our study found that the effect on the HLG could vary dramatically based on substituent location.

When the armchair structure of the parent PAH is asymmetric, two non-identical armchair locations are present where ketone groups can be added to the PAH, one closer to the center of the molecule and one further from the center of the molecule. In addition, for both symmetric and asymmetric molecules, the sp^3 hybridized carbon could be located either immediately adjacent to or across the armchair from each location of the ketone group. Figure 4 shows both changes in ketone location for ketone-containing PAH with the sp^3 hybridized carbon located either across the armchair or adjacent to the ketone. Ketone-containing PAH with the sp^3 hybridized carbon located adjacent to the ketone had only minor differences in ΔHLG both overall, and when comparing changes in ketone location from the outside to the inside of an asymmetric PAH parent molecule or when on a symmetric PAH parent. Conversely, structures with the PAH located across the armchair had a very large range in HLG compared to that of the parent molecule, as seen by the extremely large standard deviations for these structures in Fig. 4. The

Please cite this article as: J.A. Giaccai, J.H. Miller, Examination of the electronic structure of oxygen-containing PAH dimers and trimers, Proceedings of the Combustion Institute (2018), https://doi.org/10.1016/j.proci.2018.05.057

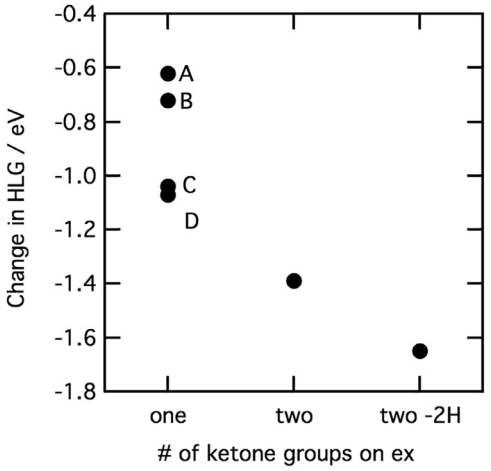

Fig. 5. Change in HLG as the number of ketone moieties on the PAH increases. Two non-identical locations for the ketone moiety and two locations for the sp3 carbon account for the four data points with one carbonyl group on the PAH; conformations A-D can be seen in Fig. S4. Dehydrogenation of the double ketone PAH to a quinone-like structure is shown in a separate column. The parent molecule is dinaphtho(8,1,2-abc:2′,1′,8′-klm)coronene.

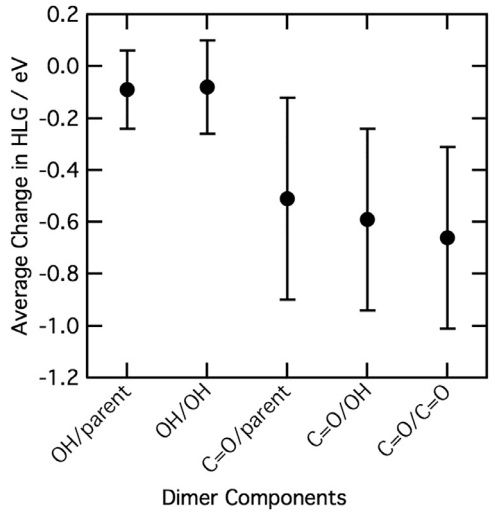

Fig. 6. Average ΔHLG from the parent-parent dimer with the increase in number of ketones present in dimer for all molecules examined. Error bars show standard deviation in ΔHLG over the various PAH parent molecules examined.

hydrogen atoms on the sp^3 carbon in these molecules are very close to the oxygen and can easily form a keto-enol structure with the ketone group. Although the structures of the molecules were confirmed after geometry optimization, slight differences in hydrogen proximity to the oxygen may result in the variations of ΔHLG observed.

The variation in HLG with a change in oxygen location on the parent PAH molecule also can be seen in the extended armchair structure of dinaphtho(8,1,2-abc:2′,1′,8′-klm)coronene [ex]. In dinaphtho(8,1,2-*abc*:2′,1′,8′-*klm*)coronene, four possible molecular configurations to add a single ketone group were studied, conformations A-D, see Fig. S4, as well as the addition of a second ketone group. Figure 5 shows two groupings of two data points each where only one ketone was added to the dinaphthocoronene. The range in ΔHLG over the variations in the molecular structure demonstrates how important the exact location of the ketone group is to the HLG. As observed previously, the structures with the sp^3 carbon adjacent to the ketone, A and B, show a smaller decrease in HLG than the structures with the sp^3 carbon located across the armchair from the ketone, C and D.

As Chen and Wang found [18], multiple oxygens on a PAH molecule increase the effect on the HLG. In situations where little effect was caused by the original oxygen moiety, e.g., a hydroxyl substituent, little effect was observed when multiple substituents were added to the PAH. However, molecules with more than one ketone group added (to different aromatic rings of the PAH molecule) demonstrated a larger decrease in HLG with each subsequent addition, see Fig. 5. When an even number of carbonyls are added to a PAH, dehydrogenation of the two sp^3 carbons paired with the ketone additions results in a quinone-like structure. The number of π electrons present is not only those in the original PAH structure, but also the lone pairs from the oxygen in the ketone moiety and an additional pair of electrons from the new double bond due to the dehydrogenation. The presence of quinone-like structures further decreases the band gap, beyond that observed by the addition of two ketone groups. This strongly suggests that the change in aromaticity with addition of the carbonyl groups onto the PAH is what brings about the largest decrease in HLG.

3.2. Oxygen-containing PAH dimers and trimers

Two series of dimers were studied. In the first study hydroxyl/hydroxyl, hydroxyl/parent, ketone/hydroxyl, ketone/parent and ketone/ketone dimers were compared to parent/parent dimers for all the PAH in this study, with all of the monomers containing only one oxygen moiety. Figure 6 shows that there is no significant difference in HLG between hydroxyl/ketone, ketone/parent molecule, and ketone/ketone dimers. The two dimers with oxygen present but no ketone moiety all have similar HLG, while the three dimers with one or more ketone-containing monomer have an average ΔHLG from non-ketone-containing dimers of

Please cite this article as: J.A. Giaccai, J.H. Miller, Examination of the electronic structure of oxygen-containing PAH dimers and trimers, Proceedings of the Combustion Institute (2018), https://doi.org/10.1016/j.proci.2018.05.057

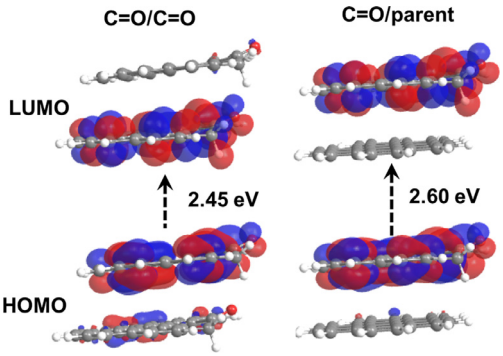

Fig. 7. Molecular orbitals for ketone-ketone and ketone-parent dimers showing electron density remains on the ketone containing monomer in the HOMO and LUMO orbitals. In the ketone/parent dimer the ketone molecule is the upper molecule. Parent molecule is naphtha[8,1,2-*abc*]coronene.

−0.5 eV, whether the dimer has a total of two or only one carbonyl group.

Examination of the molecular orbitals of the mixed dimer, Fig. 7, demonstrates that electron density is concentrated on the ketone-containing monomer in the ketone/parent dimer, whereas in the ketone/ketone dimer, the electron density is located on both molecules between the HOMO and LUMO, as found in homogeneous PAH dimers in earlier studies [20]. In the HOMO both molecules have some electron density, although the main components of the HOMO are located on the upper molecule of the dimer, whereas the electron orbitals comprising the LUMO are primarily from the lower molecule of the dimer pair. This is in contrast to the ketone/parent dimer where the electron density for both the HOMO and LUMO is only present on one molecule, the ketone-containing PAH.

The second series of dimers paired hydroxyl– and ketone-containing PAH with circumcoronene (cc). In earlier studies [20], dimers formed from one large and one small PAH had a HLG close to that of the larger molecule, until the molecules approach a similar size, when there is a decrease in the HLG. Figure 8 demonstrates that the lowest HLG of the two monomers controls the HLG of the dimer, not necessarily monomer size. When molecules with a larger HLG than circumcoronene are paired with circumcoronene, the HLG of the dimer is close to the lower HLG of circumcoronene, demonstrated by the HLG of dimer pairs that reach an asymptote at the HLG of circumcoronene, Fig. 8a. The HLG of the dimer diverges from the asymptote when molecules with HLG lowered by ketone groups, or even more so, dehydrogenated molecules with more than one ketone and a quinone-like structure begin to dominate the HLG of the dimer pair. Figure 8b–d illustrates the molecular orbitals found for the different dimer situations. When the HLG of the dimer is dominated by that of the ketone-containing monomer, electron density remains on the ketone-containing monomer, Fig. 8b; when the HLG of the dimer is dominated by the circumcoronene monomer, electron density remains on the circumcoronene molecule, Fig. 8d. Where the HLG of both monomers is similar, the electron orbitals of the individual monomers overlaps and electron density is found on both molecules of the dimer in the HOMO and LUMO.

In the limited number of trimer systems studied, the same effects observed in dimers remain. Trimers with the lowest bandgap were observed when they contained molecules with more than one ketone group. If two of the ketone-containing PAH were next to each other the electron density could spread across both molecules, as in the dimer in Fig. 7, and further lowers the HLG.

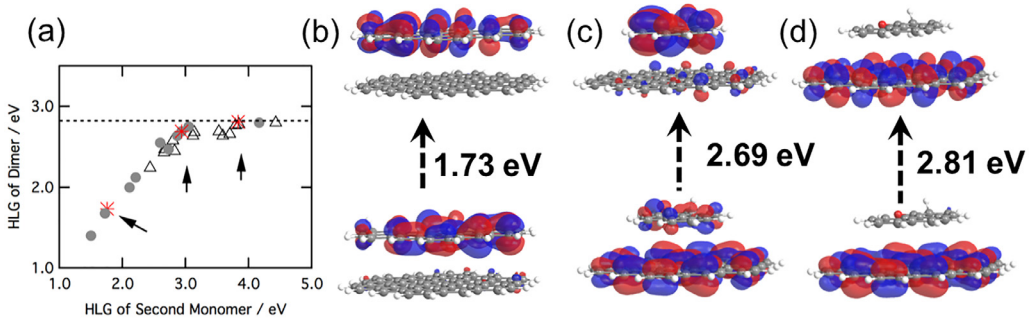

Fig. 8. (a) Comparison of HLG between monomers and dimers formed with circumcoronene. Dashed line: HLG of circumcoronene monomer, circles: ketone-containing PAH, triangles: non-ketone containing PAH, stars: dimers illustrated in molecular orbitals, indicated by arrows. Molecular orbital diagrams of the LUMO (top row) and HOMO (bottom row) for three dimers. In (b) the electron density remains on the lower HLG ketone-containing PAH, in (d) the electron density remains on the lower HLG circumcoronene, and in (c) the HLG of both monomers are similar and electron density is on both molecules. Circumcoronene molecule is the lower molecule in all dimers.

Please cite this article as: J.A. Giaccai, J.H. Miller, Examination of the electronic structure of oxygen-containing PAH dimers and trimers, Proceedings of the Combustion Institute (2018), https://doi.org/10.1016/j.proci.2018.05.057

4. Conclusions

Understanding the effect of different molecular structures on the HLG of PAH molecules and agglomerates is important in being able to properly interpret analyses of soot and PAH molecules both in samples of soot emitted from flames and in situ measurements. In areas where oxygen reactions with nascent soot can be expected, unless the presence of ketones is suggested, the effect on HLG of the PAH should be minimal. However, in later stages of soot development, and in post-combustion atmospheric oxidation of soot where ketones are more common, a decrease in HLG should be expected. The decrease in band gap with oxygen-containing PAH is separate from other effects on band gap, so it may be combined with changes in PAH topology and aggregation to further decrease the band gap. Those interested in designing PAH-based solar cells and quantum computers may find these effects particularly useful. The quinone-like structures studied had HLG approaching 2–1.5 eV, or 620–830 nm in the red and near infrared areas of the solar spectrum. The lower HLG of quinones and quinone-like PAH found in soot particles that have been oxidized atmospherically will affect the amount of radiative forcing occurring in the atmosphere and should be better understood to predict the role of soot and oxidized soot in climate change. Further experimental studies of the oxidation during the later stages of soot formation and in the atmosphere for different combustion sources are required to give an accurate description of the types of oxidation occurring in atmospheric soot and to allow an accurate prediction for the role of oxidized PAH.

Acknowledgments

This material is based upon work supported by the U.S. National Science Foundation under grant no. CBET- 1706757 with Song-Charng Kong serving as technical monitor. Support for J.A.G. was provided by the David G. White Fellowship. NWChem calculations were performed on George Washington University's high-performance computing cluster, Colonial One.

Supplementary materials

Supplementary material associated with this article can be found, in the online version, at doi: 10.1016/j.proci.2018.05.057.

References

[1] R.C. Moffet, K.A. Prather, *Proc. Natl. Acad. Sci. USA* 106 (2009) 11872–11877.
[2] P.G. Luo, S. Sahu, S.-T. Yang, et al., *J. Mater. Chem. B* 1 (2013) 2116–2127.
[3] A. Barradas-Gimate, M.A. Murillo-Tovar, J. de J. Díaz-Torres, et al., *Atmosphere* 8 (2017) 140.
[4] M.E. Schuster, M. Hävecker, R. Arrigo, et al., *J. Phys. Chem. A* 115 (2011) 2568–2580.
[5] R.L. Vander Wal, V.M. Bryg, *Chemistry Characterization of Jet Aircraft Engine Particulate by XPS: Results from APEX III, NASA/CR—2014-218293*, National Air and Space Administration, 2014.
[6] R.L. Vander Wal, V.M. Bryg, M.D. Hays, *Anal. Chem.* 83 (2011) 1924–1930.
[7] D.J. Growney, O.O. Mykhaylyk, L. Middlemiss, et al., *Langmuir* 31 (2015) 10358–10369.
[8] F.-X. Ouf, et al., *Sci. Rep.* 6 (2016) 36495, doi:10.1038/srep36495.
[9] K.O. Johansson, T. Dillstrom, M. Monti, et al., *Proc. Natl. Acad. Sci. USA.* 113 (2016) 8374–8379.
[10] K.O. Johansson, F. El Gabaly, P.E. Schrader, M.F. Campbell, H.A. Michelsen, *Aerosol Sci. Technol.* (2017) 1–12.
[11] D.E. Edwards, D.Y. Zubarev, W.A. Lester, M. Frenklach, *J. Phys. Chem. A* 118 (2014) 8606–8613.
[12] X. You, D.Y. Zubarev, W.A. Lester, M. Frenklach, *J. Phys. Chem. A* 115 (2011) 14184–14190.
[13] D.E. Edwards, X. You, D.Y. Zubarev, W.A. Lester, M. Frenklach, *Proc. Combust. Inst.* 34 (2013) 1759–1766.
[14] R. Singh, M. Frenklach, *Carbon* 101 (2016) 203–212.
[15] R.I. Singh, A.M. Mebel, M. Frenklach, *J. Phys. Chem. A* 119 (2015) 7528–7547.
[16] S.V. Chaparala, A. Raj, *Combust. Flame* 165 (2016) 21–33.
[17] D. Chen, H. Wang, Electronic properties of polycyclic aromatic hydrocarbons and their derivatives, *10th US National Combustion Meeting*, 2017.
[18] E.M. Adkins, J.H. Miller, *Phys. Chem. Chem. Phys.* 19 (2017) 28458–28469.
[19] E.M. Adkins, J.A. Giaccai, J.H. Miller, *Proc. Combust. Inst.* 36 (2017) 957–964.
[20] J.H. Miller, J.D. Herdman, C.D.O. Green, E.M. Webster, *Proc. Combust. Inst.* 34 (2013) 3669–3675.
[21] M. Valiev, E.J. Bylaska, N. Govind, et al., *Comput. Phys. Commun.* 181 (2010) 1477–1489.
[22] R. Krishnan, J.S. Binkley, R. Seeger, J.A. Pople, *J. Chem. Phys.* 72 (1980) 650–654.
[23] K. Kim, K.D. Jordan, *J. Phys. Chem.* 98 (1994) 10089–10094.
[24] P.J. Stephens, F.J. Devlin, Cf. Chabalowski, M.J. Frisch, *J. Phys. Chem.* 98 (1994) 11623–11627.
[25] J.H. Miller, W.G. Mallard, K.C. Smyth, *J. Phys. Chem.* 88 (1984) 4963–4970.
[26] J.D. Herdman, J.H. Miller, *J. Phys. Chem. A* 112 (2008) 6249–6256.
[27] D.E. Williams, *J. Comput. Chem.* 22 (2001) 1154–1166.
[28] J. Giaccai, E.M. Adkins, J.H. Miller, Computations of Physical and Electronic Structure of Stacks of Polynuclear Aromatic Hydrocarbons of Varying Topologies, *10th US National Combustion Meeting*, 2017.
[29] M. Rapacioli, F. Calvo, F. Spiegelman, C. Joblin, D.J. Wales, *J. Phys. Chem. A* 109 (2005) 2487–2497.
[30] Y. Zhao, D.G. Truhlar, *J. Phys. Chem. C* 112 (2008) 4061–4067.

Please cite this article as: J.A. Giaccai, J.H. Miller, Examination of the electronic structure of oxygen-containing PAH dimers and trimers, Proceedings of the Combustion Institute (2018), https://doi.org/10.1016/j.proci.2018.05.057

[31] C. Feng, C.S. Lin, W. Fan, R.Q. Zhang, M.A.V. Hove, *J. Chem. Phys.* 131 (2009) 194702.
[32] R. Podeszwa, *J. Chem. Phys.* 132 (2010) 044704.
[33] T.S. Totton, A.J. Misquitta, M. Kraft, *J. Phys. Chem. A* 115 (2011) 13684–13693.
[34] T. Janowski, P. Pulay, *J. Am. Chem. Soc.* 134 (2012) 17520–17525.
[35] K. Rohini, D.M.R. Sylvinson, R.S. Swathi, *J. Phys. Chem. A* 119 (2015) 10935–10945.
[36] T.S. Totton, A.J. Misquitta, M. Kraft, *J. Chem. Theory Comput.* 6 (2010) 683–695.

Please cite this article as: J.A. Giaccai, J.H. Miller, Examination of the electronic structure of oxygen-containing PAH dimers and trimers, Proceedings of the Combustion Institute (2018), https://doi.org/10.1016/j.proci.2018.05.057